# Remote Sensing of Aboveground Carbon in Subtropical Thicket

GEF-5 SLM Project

Baviaanskloof Component, South Africa

November 2019

Dugal Harris, Cosman Bolus and James Reeler

**Author contact details:**

Dugal Harris
Earth observation consultant

Tel: +27 82 843 9679
Email: dugalh@gmail.com

Cosman Bolus
Sustainable Landscape Services

Tel: +27 78 002 6726
Email: cosbolus@gmail.com

James Reeler
WWF South Africa

Tel: +27 21 657 6600
Email: jreeler@wwf.org.za

**Correspondence address:**

Rebecca Powell
Project coordinator: GEF5 Sustainable Land Management Project, Eastern Cape
Environmental Science Department, Rhodes University

Tel: +27 46 603 7005
Email: rebeccajoub@gmail.com

**Suggested citation:**

Harris, D., Bolus, C., Reeler, J. 2019. Remote sensing of aboveground carbon in subtropical thicket, GEF-5 SLM, Rhodes University. Internal report. https://www.doi.org/10.13140/RG.2.2.35106.96961/1

# Summary

High spatial resolution maps of aboveground carbon (AGC) will assist with the monitoring and verification of carbon stored through restoration of subtropical thicket. Field methods are required for capturing AGC ground truth data at the plot scale, but are highly impractical for large area mapping of carbon stocks. Against this background, a remote sensing method to estimate AGC from multi-spectral imagery was developed. The technique and associated data analyses contribute to outcome 3.1 ("Government approved methodology developed for the generation of carbon credits through restoration of spekboomveld"), of the GEF-5 SLM ("Securing multiple ecosystems benefit through SLM in the productive but degraded landscapes of South Africa") project. AGC ground truth was acquired for 90 plots in a small study area in the Baviaanskloof, South Africa. Using the ground truth, univariate and multivariate snapshot models were developed to predict AGC from features in a 2017 WorldView-3 (0.34 m resolution 8-band) satellite image. Informative features were selected from a large set of spectral, textural and vegetation index features using stepwise forward selection. Using this approach, the multivariate model produced a coefficient of determination ($R^2$) of 0.92 and root mean square error (RMSE) of 2.48 t C $ha^{-1}$. In addition to the snapshot models, a simple calibration method was devised to facilitate the generation of repeat AGC maps of the study area. The method uses a linear transform, fitted to invariant image areas, to calibrate suitable features in new images. Experiments conducted on a multi-temporal images (consisting of two WorldView-3 images and one 0.5 m resolution 4-band aerial image mosaic) demonstrated the potential of the approach. Mean $R^2$ and RMSE statistics of the calibrated models were 0.79 and 5.25 t C $ha^{-1}$ respectively. This study shows the efficacy of regression approaches for estimating AGC from multi-spectral imagery, and provides a foundation for the spatial and temporal extension of AGC remote sensing in the thicket biome. The remote sensing method is suitable for inclusion under the AR-ACM0003 CDM (Clean Development Mechanism) carbon accounting methodology.

# Table of Contents

# Table of Figures

# 1 Introduction

## 1.1 Restoration of subtropical thicket

The subtropical thicket biome occurs in the southern and south-eastern parts of South Africa (Vlok & Euston-Brown 2002) and is characterised by a dense and diverse combination of small trees, thorny shrubs, grasses and succulents (Cowling, ProcheÕ & Vlok 2005). Figure 1.1 shows an example of an arid thicket habitat in the Little Karoo. Degradation of this biome, caused by poorly managed goat browsing, is associated with severe reductions in biodiversity and ecological functioning (Lechmere-Oertel, Kerley & Cowling 2005; Lloyd, Van den Berg & Palmer 2002; Mills et al. 2005). It is estimated that 90% of the thicket biome has suffered moderate to severe degradation of this form (Lloyd, Van den Berg & Palmer 2002; Thompson et al. 2009). Degraded habitats appear to follow a trajectory of increasing desertification (Lechmere-Oertel, Kerley & Cowling 2005), and do not recover after removal of livestock (Sigwela et al. 2009). Active measures are required to restore ecosystem health.

Figure 1.1 Arid thicket in the Little Karoo, with spekboom in the foreground

Restoration of degraded thicket is a topic of ongoing research. Studies at established restoration sites have suggested that planting of spekboom (*Portulacaria afra*) is a viable means for large-scale thicket restoration (Mills & Cowling 2006; Powell, Mills & Marais 2005). The use of spekboom in restoration is motivated by its role as a dominant and keystone thicket species (Lechmere-Oertel et al. 2008; Van der Vyver et al. 2013). Spekboom is also unusually effective at sequestering carbon for an arid region plant (Mills & Cowling 2006), which has obvious significance in the context of climate change mitigation. Comparisons of intact and degraded thicket indicate that restoration stands to capture about 30 t C $ha^{-1}$ in above ground carbon (AGC) across the biome (Van der Vyver & Cowling 2019). Evaluation of the Thicket-wide Plot restoration experiments have shown an AGC accrual rate of 2.3 t C $ha^{-1}$ $yr^{-1}$ to be a viable restoration target (M L. Van der Vyver 2017). Approximately 1.7 million ha of thicket is suitable for restoration via spekboom planting (Lloyd, Van den Berg & Palmer 2002) within the biome. It should

be noted that the return of thicket biodiversity through spekboom planting remains an uncertain outcome, and this critical aspect of restoration demands further research (Powell 2009).

Spatial information is required to support the planning and monitoring of restoration. In the context of climate change, maps of above ground carbon (AGC), an important indicator of ecosystem health, are of particular interest (Clarke, Shackleton & Powell 2012; Mills et al. 2010; Powell 2009). Carbon stored through restoration can be verified and traded on the carbon market, providing a source of restoration funding (Marais, Cowling & Powell 2009; Mills et al. 2007). This trade is facilitated by organisations such as Verified Carbon Standard (VCS) and Climate Community and Biodiversity Alliance (CCBA) who audit carbon accounting and environmental practice (Mills & Cowling 2014). Verified carbon credits can be purchased by countries or corporations wishing to offset their carbon emissions (they may want to do this voluntarily, to meet carbon tax requirements or to satisfy international agreements such as the Kyoto Protocol and Paris Agreement). To date, 4.7 million ex ante carbon credits have been generated under VCS and CCBA by two thicket restoration projects (Mills et al. 2015). However, none of these credits have been sold as yet, and the public sector project has missed a critical timeline point for verification of credits, such that the project will need re-validation before it can generate credits. This illustrates some of the challenges experienced in bringing such credits to market.

Destructive sampling and allometric approaches, involving harvesting and per-plant measurements, are typically used for quantifying carbon stocks in the field (Lu et al. 2016; Powell 2009; Van der Vyver & Cowling 2019). These approaches are known to be time-consuming and costly, and are highly impractical for large scale carbon stock mapping (Eisfelder, Kuenzer & Dech 2012; Lu 2006). This is especially true in the thicket biome due to rugged terrain, dense vegetation and complex growth forms (Powell 2009; Van der Vyver & Cowling 2019). A remote sensing approach for AGC mapping in thicket would therefore be of great assistance in the monitoring and auditing of carbon stocks generated through restoration. Repeat AGC maps would also be useful for deepening the current understanding of thicket ecosystem dynamics (Eisfelder, Kuenzer & Dech 2012).

## 1.2 Remote sensing of biomass

Various forms of light detection and ranging (LiDAR), synthetic aperture radar (SAR) and optical (multi-spectral and hyperspectral) data have been used (independently or in combination) for remote sensing of biomass (Lu et al. 2016). LiDAR data provides information on the three-dimensional spatial structure of vegetation (Eisfelder, Kuenzer & Dech 2012). Given the known correlation between vegetation spatial dimension and biomass (Van der Vyver & Cowling 2019), LiDAR has obvious application for biomass estimation. Being an active sensor, LiDAR is not affected by time of capture or sun position (Ali et al. 2015), which simplifies its use in repeat mapping applications. Very high spatial resolution (VHSR) LiDAR is however costly and limited in coverage (Ali et al. 2015). Its suitability for use in short-stature vegetation is hampered by difficulties in separating canopy from ground returns, and relatively low penetration of dense canopies (Kulawardhana, Popescu & Feagin 2017), such as those of intact subtropical thicket.

SAR data is frequently used for biomass mapping, especially in forested areas (Lu et al. 2016). SAR can operate independent of weather and has global coverage (Ali et al. 2015). Longer electromagnetic wavelengths are capable of penetrating into the canopy (Goetz et al. 2009) and backscatter is influenced by biomass, but also by other factors such as topography and soil moisture (Eisfelder, Kuenzer & Dech 2012; Mathieu et al. 2018). Commercial satellites, such as TerraSAR-X, offer shorter wavelength X-band

SAR data at VHSR (ESA 2007). Longer L band wavelengths are the most frequently used for vegetation mapping, however, because of their ability to penetrate the canopy (Eisfelder, Kuenzer & Dech 2012; Lu et al. 2016; Mathieu et al. 2018). Spatial resolution of SAR data in this band is necessarily coarse (e.g. 7 – 100 m for ALOS PALSAR), and not suitable for direct use with small ground truth plots. SAR can suffer from saturation in high biomass (100 to 150 t C ha-1) habitats, such as tropical forest (Goetz et al. 2009), although this problem is slightly alleviated through the use of interferometry SAR (InSAR) (Lu et al. 2016). Saturation seems unlikely to occur with the modest AGC figures of thicket, but this is untested.

Optical reflectance in the visible, near-infrared (NIR) and short-wave infrared (SWIR) bands is affected by vegetation structure and photosynthetic activity, and is indirectly correlated with biomass (Eisfelder, Kuenzer & Dech 2012; Lu et al. 2016). Optical satellite data is cost-effective, has global coverage, and is increasingly available in a variety of spectral and spatial resolutions. Drawbacks of optical data are its dependence atmospheric conditions and viewing geometry (anisotropy) (Mather & Koch 2011), and its lack of sensitivity to the vertical dimension i.e. vegetation height.

In the majority of cases, carbon stocks are estimated using regression models that describe empirical relationships between features (i.e. variables) derived from remote sensing data and carbon stock ground truth (Ali et al. 2015; Lu et al. 2016). In some LiDAR studies, a more theoretical approach is used where variables such as canopy height and area can be measured directly (Kulawardhana, Popescu & Feagin 2017). With optical data, features used include vegetation indices, band ratios and texture descriptors (Eisfelder, Kuenzer & Dech 2012; Lu 2006). Regression methods are divided into parametric and non-parametric types. Parametric approaches assume a model structure *a priori* and use the data to estimate the parameters of this model (e.g. linear regression). In non-parametric approaches, the model structure is effectively learnt from the data and no assumptions about the form of the underlying relationships are made (Jain, Duin & Mao 2000). The non-parametric approach is suited to cases where the underlying model is complex and non-linear, as these relationships are seldom known in advance. However, as a general rule, the non-parametric approach requires more data for representative fitting (Lu et al. 2016), and the parametric approach is better suited to limited ground truth data sets.

## 1.3 Remote sensing of subtropical thicket

Thompson et al. (2009) produced a degradation map of the biomes occurring in the Little Karoo. Using the vegetation map of Vlok, Cowling & Wolf (2005), different models were developed for four habitat types (Gannaveld, Apronveld, Succulent Karoo-thicket mosaic and Spekboom thicket). A straightforward thresholding approach, using 250 m resolution MODIS normalised difference vegetation index (NDVI) data, was used for mapping degradation in thicket. The study was successful at estimating three degradation levels (intact, moderate and severe) of spekboom thicket.

A method for estimating AGC in subtropical thicket was devised by Nyamugama & Kakembo (2015) using SPOT 5 10 m spatial resolution imagery and a set of 90 30 m × 30 m carbon stock ground truth plots. A univariate quadratic regression model was fitted using a SPOT-5 NDVI feature (dependent variable) which achieved $R^2$ values of 0.975, 0.812 and 0.725 for intact, transformed and degraded classes respectively. The SPOT-5 model was subsequently applied unmodified to a time series of Landsat NDVI, to estimate change in carbon stocks over the period 1972-2010. Time series results were not validated, but showed a marked decrease in AGC over time.

Bayer et al. (2016) developed a method for mapping soil organic carbon (SOC) with airborne hyperspectral data. SOC was related to spectral features in field spectroscopic data using a regression approach. Airborne HyMap hyperspectral data (126 bands and 3.3 m spatial resolution) of a small study area was pre-processed using spectral mixture analysis (SMA) to remove the influence of vegetation in mixed pixels. The field model was then be applied to the residual (unmixed) soil spectra to produce a SOC map.

A method for regional mapping of spekboom canopy cover was developed by Harris, Vlok & Van Niekerk (2018). Multi-spectral VHSR aerial imagery from National Geo-spatial Information (NGI) (National Geo-spatial Information 2012) of a large region in the Little Karoo was corrected for spatially varying atmospheric and anisotropic effects using a radiometric homogenisation procedure (Harris & Van Niekerk 2019). Feature clustering and ranking (FCR) (Harris & Van Niekerk 2018) was applied to select an informative set of features from a high dimensional set of spectral, vegetation index and texture features. A supervised classification (decision tree) approach was subsequently applied to the reduced feature set, to produce the canopy cover map.

## 1.4 Contribution to the GEF-5 SLM project

This report presents the development and evaluation of techniques for the remote sensing of AGC in subtropical thicket. The research contributes to outcome 3.1, i.e. “Government approved methodology developed for the generation of carbon credits through restoration of spekboomveld”, of the GEF-5 “Securing multiple ecosystems benefit through SLM in the productive but degraded landscapes of South Africa” (SLM) project (GEF 2013).

Practical constraints of budget, known challenges of using LiDAR in short stature habitats (Kulawardhana, Popescu & Feagin 2017), and a lack of established methods in semi-arid habitats (Eisfelder, Kuenzer & Dech 2012), meant that SAR and LiDAR were not considered in this study. WorldView-3 8-band imagery of a small (3000 ha) study site in the Baviaanskloof was the principal source of data for the technique. Multi-spectral imagery has been used successfully in related studies in thicket (Harris, Vlok & Van Niekerk 2018; Nyamugama & Kakembo 2015). The WorldView-3 imagery provides four bands in the red-infrared spectral region which is known to be informative for vegetation characterisation (Fassnacht et al. 2016). The high WorldView-3 spatial resolution of 0.34 m facilitated the use of features describing vegetation texture and allowed detailed coverage of small (10 m × 10 m) ground truth plots.

A set of typical vegetation index, band ratio and texture features (and non-linear transformations thereof) were generated from the imagery and reduced to an informative minimum using a stepwise forward selection approach (Jain, Duin & Mao 2000). Univariate and multivariate linear regression models were subsequently fitted to selected features and evaluated with AGC ground truth data comprised of 90 plots. Experiments were conducted to investigate the efficacy of a technique for temporally transferring AGC models to repeat images of the study area. The temporal calibration technique made use of a linear calibration transform fitted to data from areas of invariant land cover. Lastly, the relationship between vegetation volume and AGC was investigated as a preliminary step to inform future remote sensing research in the biome.

# 2 Methods

## 2.1 Study site

The study area is spread over the farms Sewefontein, Tchnuganoo and Beacosnek, in the central Baviaanskloof, South Africa (see Figure 2.1). Subtropical thicket, fynbos and renosterveld vegetation types are all found in the study area (Skowno & Euston-Brown 2006). Spekboom thicket on the mid to lower slopes in this area has been severely degraded by over-browsing. The less accessible, and more rugged upper slopes in the western Beacosnek section contain areas of intact and moderately degraded thicket. Spatial extent of the thicket habitat and its degradation classes are shown in in Figure 2.2.

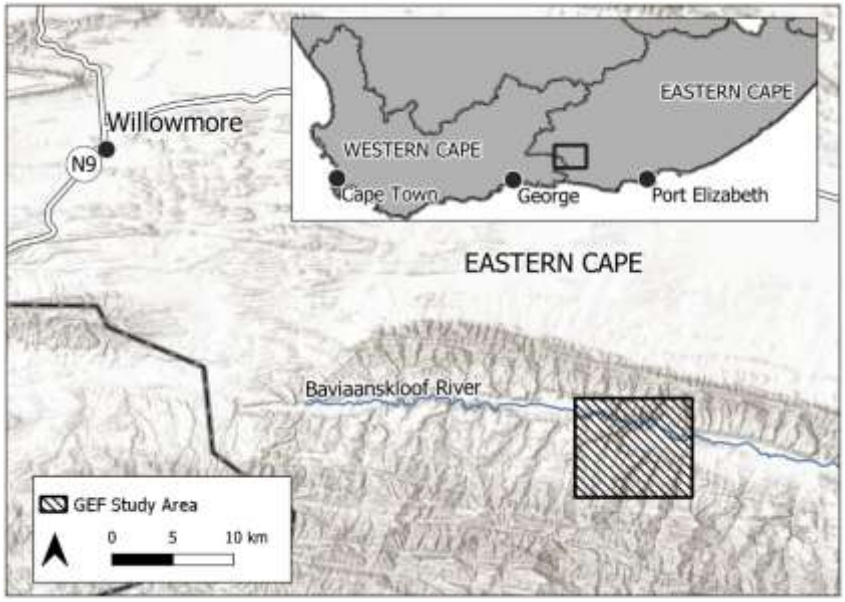


*Figure 2.1 Study area context map*

## 2.2 Data

Three images of the study area were obtained, consisting of two WorldView-3 0.34 m 8-band satellite images, and one 0.5 m 4-band stereo aerial mosaic from NGI (National Geo-spatial Information 2012). Details of the imagery are shown in Table 2.1. A set of 30 ground control points (GCPs) of clearly distinguishable ground features were gathered in situ with a differential global positioning system (DGPS) device and post-processed to 20 cm accuracy. Using the GCPs in combination with the NGI 2015 stereo imagery, a VHSR (0.5 m) digital surface model (DSM) was produced with the Agisoft Photoscan (Agisoft 2019) photogrammetry application. The GCP locations and DSM are shown in Figure 2.2. Using the GCPs and DSM, the WV3 2017 image was orthorectified to sub-meter accuracy, and subsequently corrected for atmospheric effects using ATCOR-3 (Richter 1997), and pan-sharpened to 0.34 m spatial resolution. The WV3 2018 image and NGI 2015 images were orthorectified using automatic GCP generation with the WV3 2017 orthorectified image as reference. The orthorectified NGI 2015 mosaic was radiometrically corrected using radiometric homogenisation (Harris & Van Niekerk 2019) with a concurrent and collocated MODIS MCD43A4 product as surface reflectance reference. As key orbital and view geometry metadata were not available for the WV3 2018 image, it could not be atmospherically corrected.

*Table 2.1 Imagery details*

| Abbreviation | Source | Spatial resolution | Spectral bands | Component images | Date | Image nadir | Sun elevation |
|---|---|---|---|---|---|---|---|
| **WV3 2017** | WorldView-3 | 0.34 m | 8 | 1 | 2017/10/01 | 16.9° | 53.7° |
| **WV3 2018** | WorldView-3 | 0.34 m | 8 | 1 | 2018/11/25 | 15.9° | 68.0° |
| **NGI 2015** | NGI aerial | 0.50 m | 4 | 4 | 2015/04/27 | -5.0° – 5.0° | >30.0° |

Plant allometric measurements and litter samples were gathered in a series of field sampling exercises between December 2017 and March 2019 (Bolus et al. 2020). A total of 90 sampling plots were spread over intact, moderate and severe thicket degradation strata in a stratified random sampling approach. Severely degraded areas suitable for restoration by spekboom planting were mapped in situ by Vlok (2017). Intact and moderate degradation thicket strata were subsequently added to this map by visual delineation of the WV3 2017 image. Stratified random sampling helped ensure ground truth representivity of the range of carbon stocks present in the landscape. Based on the rule-of-thumb that one needs approximately ten times the number of data points as there are features in the model (Jain, Duin & Mao 2000), the sample size of 90 plots allows for fitting of a reasonably complex model, and falls in the upper range of similar studies (Fassnacht et al. 2014). The location of the sampling plots and spatial extents of the degradation classes are shown in Figure 2.2 against a background of the VHSR DSM.

Plot sizes were chosen as 10 m × 10 m for the moderate and intact classes, and as 20 m × 20 m for the more sparsely vegetated degraded class based on previous work (Powell 2009). While larger plot sizes are associated with improved estimation accuracy, reduced variability, and decreased sensitivity to spatial inaccuracy (Frazer et al. 2011), these benefits need to traded off against the time and cost of field measurements. A nested plot design was adopted, where all vegetation was measured in a small 5 m × 5 m subplot, and only vegetation over 0.5 m high was measured in the remainder of the containing plot. The nested plot design reduces field work while having minimal impact on AGC estimation accuracy (Lackmann 2011). Plot corners were recorded with a DGPS device and post-processed to ±30 cm accuracy. The detrimental effects of the modest plot sizes were somewhat mitigated by the high spatial accuracy of the orthorectified images and AGC plot locations, in addition to the high spatial resolution of the images (which gave a coverage of ±850 WorldView-3 pixels for the 10 m × 10 m plots). Table 2.2 contains details of area, number of plots and plot size per stratum. Appendix A documents an earlier study that used data from trial plots to inform the sampling approach and plot design. Further details of the field data and sampling approach can be found in Bolus et al. (2018) and Bolus et al. (2020).

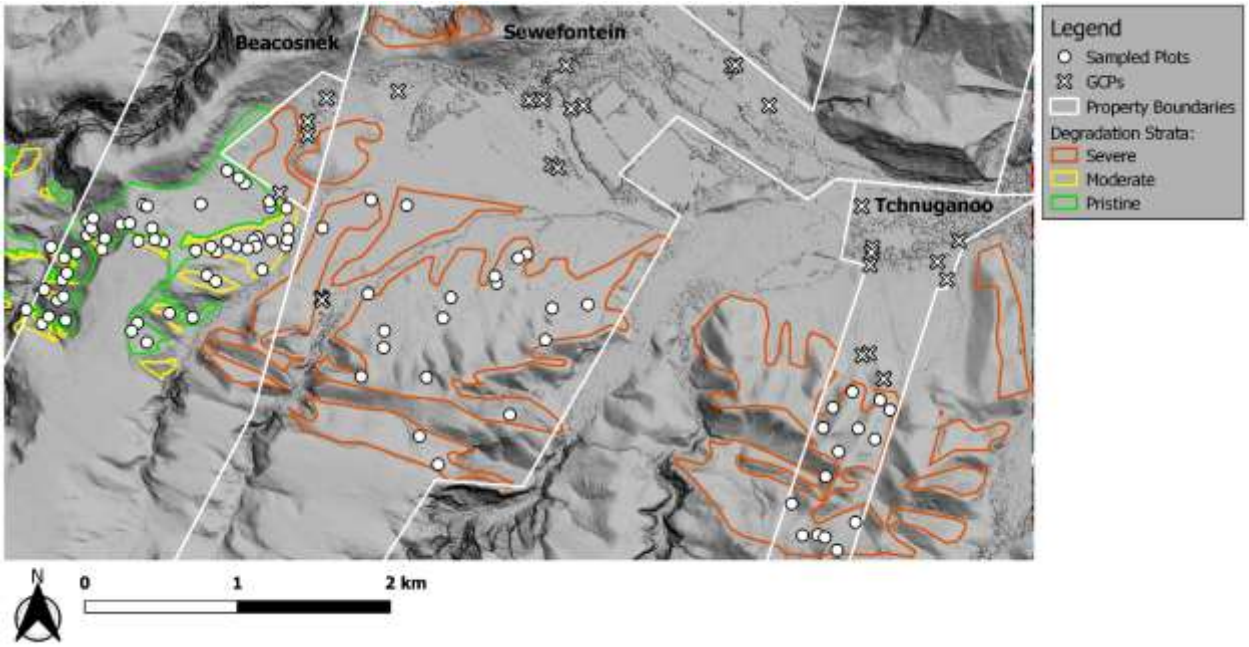


*Figure 2.2 Study area thicket degradation strata and sampled plots*

*Table 2.2 Stratified random sampling details*

| Degradation stratum | Area (ha) | Number of plots | Nested / containing plot size (m) |
|---|---|---|---|
| Intact | 78 | 29 | 5×5 / 10×10 |
| Moderate | 37 | 26 | 5×5 / 10×10 |
| Severe | 442 | 35 | 5×5 / 20×20 |
| **Total** | **557** | **90** | |

Aboveground biomass carbon (ABC) was estimated for each plot with species-specific allometric models from Van der Vyver & Cowling (2019) and wet/dry ratios from Powell (2009). The allometric models are based on crown diameter and height exclusively, and do not require basal stem diameters which are problematic and time-consuming measurements in thicket (Powell 2009; Van der Vyver & Cowling 2019). Where sampled species had no available allometric data or wet/dry ratio, parameters from a surrogate species of similar genus or growth form were used. Details of the surrogate species map are given in Bolus et al. (2020). ABC for vegetation under 0.5 m high in the containing plot was extrapolated from the 5 m × 5 m nested plot. Aboveground carbon (AGC) was then found as the sum of the ABC and Litter C plot components, and extrapolated to per hectare values.

## 2.3 Snapshot AGC regression model

Linear regression models were built and evaluated on features from the WV3 2017 image and the AGC sampling plot data.

### 2.3.1 Feature extraction

A large set of features incorporating band ratios, vegetation indices and texture measures were extracted from the WV3 2017 image, which consists of 8 multi-spectral bands and one panchromatic band as detailed in Table 2.3.

*Table 2.3 WorldView-3 spectral bands*

| Band number | Band name | Symbol | Wavelength (nm) |
|---|---|---|---|
| 1 | Panchromatic | $pan$ | 450 - 800 |
| 2 | Coastal | $C$ | 400 - 450 |
| 3 | Blue | $B$ | 450 - 510 |
| 4 | Green | $G$ | 510 - 580 |
| 5 | Yellow | $Y$ | 585 - 625 |
| 6 | Red | $R$ | 630 - 690 |
| 7 | Red-Edge | $RE$ | 705 - 745 |
| 8 | NIR1 | $NIR1$ | 770 - 895 |
| 9 | NIR2 | $NIR2$ | 860 - 1040 |

Generated features included ratios of all pair-wise band combinations:

$$BR_{i,j} = \frac{C_i}{C_j} \qquad \text{Equation 2.1}$$

where $C_i$ are the individual bands, $i, j$ are band numbers and $i \neq j$. By including the panchromatic band in the set from which band ratios were generated, intensity normalised bands (e.g. $BR_{4,1} = R/pan$) could be extracted. These normalised features help reduce intensity variation caused by topography and anisotropy (Blauensteiner et al. 2006).

In the visible spectrum, vegetation reflectance is mainly affected by chlorophyll, which absorbs incident blue and red light while reflecting some green light, giving living vegetation its characteristic green colour (Campbell & Wynne 2011). Leaves are strongly reflective in the NIR spectrum due to scattering by internal plant structures. The sharp transition from absorption to reflectance around 700 nm is an import feature for characterising vegetation (Fassnacht et al. 2016). The normalised difference vegetation index (NDVI) aims to capture this spectral feature as a single number that is invariant to illumination intensity. The soil adjusted vegetation index (SAVI) modifies NDVI to decrease sensitivity to soil influences (Huete 1988). NDVI and SAVI are defined in Equation 2.2 and Equation 2.3 respectively. Separate NDVI and SAVI values were calculated using each of the three WorldView-3 NIR bands (i.e. red-edge, NIR1 and NIR2 as detailed in Table 2.3). Following Huete (1988), a value of 0.5 was used for $L$ in Equation 2.3.

$$NDVI_i = \frac{NIR_i - R}{NIR_i + R} \qquad \text{Equation 2.2}$$

and

$$SAVI_i = \frac{(1 + L)(NIR_i - R)}{NIR_i + R + L} \qquad \text{Equation 2.3}$$

where $NIR_i =$ Red-edge, NIR1 or NIR2 for the Worldview-3 image.

Band ratio (*BR*), *NDVI* and *SAVI* per-pixel features to were converted to scalar per-plot features using entropy, mean and standard deviation statistics. The entropy statistic describes the amount of

randomness in a variable. Entropy and standard deviation serve as basic texture features describing local spectral complexity. The entropy of the vector of sampling plot pixel values, $\boldsymbol{f}$, is defined as (Trias-Sanz, Stamon & Louchet 2008)

$$Entropy(\mathbf{f}) = -\sum_{i} h_i(\boldsymbol{f}) \log_2 h_i(\boldsymbol{f}) \qquad \text{Equation 2.4}$$

where $h_i(\boldsymbol{f})$ is the probability in the $i^{th}$ histogram bin of $\boldsymbol{f}$ (100 bins were used).

The mean and standard deviation of the *N* values in $\boldsymbol{f}$ are defined by Equation 2.5 and Equation 2.6 respectively.

$$\bar{\boldsymbol{f}} = \frac{1}{N}\sum_{i=1}^{N} f_i \qquad \text{Equation 2.5}$$

$$Std(\boldsymbol{f}) = \sqrt{\frac{1}{N-1}\sum_{i=1}^{N}\left(f_i - \bar{\boldsymbol{f}}\right)^2} \qquad \text{Equation 2.6}$$

In addition to the above features, square, square root and log functions of the mean feature values (from Equation 2.5) were included in the extracted set. A total of 522 features were generated with the above procedure.

### 2.3.2 Feature selection

For a finite number of samples, increasing the number of model features beyond a certain point results in overfitting and a decrease in regression accuracy. This so-called "peaking phenomenon" (Jain, Duin & Mao 2000) requires the size of the feature set to be reduced to a salient minimum in order to achieve accurate regression. Informative subsets of features were identified using a stepwise forward selection (FS) procedure, with the root mean square error (RMSE) of a linear model as evaluation criterion. FS starts with an empty set and proceeds in a series of steps where one feature is added to the selected set at each step (Jain, Duin & Mao 2000). The feature whose addition most improves the evaluation criterion is the one added at that step. To avoid positively biasing the RMSE criterion, it was found with five-fold cross-validation (Bishop 2003). The number of selected features for the multivariate model was chosen to minimise the RMSE criterion.

### 2.3.3 Linear regression

Multivariate and univariate linear regression models were fitted to selected features. The univariate model was included for use in the temporal transferability study, and for its relevance to spatial extension of the method. A parametric modelling approach was adopted due to the limited number of sampling plots (Ali et al. 2015). While the models are linear in the parameters, the inclusion of square root, square and log feature transformations allowed for description of non-linear relationships. The models were evaluated with leave-one-out cross validation (LOOCV) to avoid overfitting. Snapshot AGC

maps of the study area were generated by applying the univariate and multivariate models to the WV3 2017 image.

## 2.4 Temporal transferability

A major challenge in remote sensing of biomass is the transferability of mapping methods over spatial and temporal extents (Eisfelder, Kuenzer & Dech 2012; Lu et al. 2016; Lu 2006). Variations in habitat, phenology and radiometry (i.e. atmospheric and anisotropic effects) limit the extent over which remote sensing methods can be applied. A method for remote sensing of AGC in thicket should ideally allow repeat applications to new images of the same area, so that changes in AGC can be monitored over time.

Based on this background, a simple method for temporal calibration of image features was developed. A univariate linear AGC model was used for the purposes of temporal calibration method development and evaluation. The calibration method facilitates use of the AGC model on new images by applying a linear transform to the dependent variable (image feature). The image from which the model is derived is termed the *model image*, and the new image to which model is applied is termed the *calibration image*. The calibration transform expresses the relationship between image features in the *calibration* and *model* images. It is derived by linear regression on features extracted from a small set of "invariant" plots in both images. Invariant plots should be areas where the land cover has not changed over time e.g. bare soil or pristine vegetation.

A subset of informative image features were evaluated for transferability and AGC prediction accuracy. Correlation of sampling plot image features between the WV3 2017 and WV3 2018, and between WV3 2017 and NGI 2015 images were examined. In addition, the accuracy of a univariate AGC model on the WV3 2017 image was evaluated for each candidate feature. The best performing feature overall was selected for use in the univariate AGC model.

The temporal calibration approach was evaluated on the Table 2.1 images. Each image was allowed to act as the *model* image against which the other two images were calibrated. The AGC model was fitted to features from the sampling plots in the *model* image. The calibration transform was fitted to features from a random subset of 9 of the sampling plots (in the *model* and *calibration* images), and then applied to the features from all 90 plots in the *calibration* image. Finally, the AGC model was applied to the calibrated features and evaluated on the AGC ground truth. Average $R^2$ and RMSE values were found for each *model – calibration* image combination over twenty bootstraps of the above process.

These experiments assumed that AGC in the 90 sampling plots stayed approximately constant over the capture period of the images (i.e. 2015 – 2018), allowing the same AGC ground truth to be used for building models with each separate image. This assumption is a somewhat crude simplification of a complex situation, but is supported by the lack of significant disturbances to the sampled area over the capture period and the known slow AGC dynamics in thicket (Hoare et al. 2006; Van der Vyver & Cowling 2019).

## 2.5 AGC from plant volume

The potential of remotely sensed plant volume to estimate AGC was evaluated by estimating plant volume from available field allometric data and comparing to AGC measurements. Plot plant volumes were estimated using by summing the cylindrical volume for each sampled plant. The plot volume $V$, was defined as:

$$V = \sum_{k=0}^{n} \pi \left( \frac{W_k + L_k}{4} \right)^2 \cdot H_k \qquad \text{Equation 2.7}$$

where $W_k$, $L_k$ and $H_k$ are the canopy width, length and height for the $k^{th}$ plant respectively.

# 3 Results

## 3.1 Snapshot AGC regression model

The allometric models of Van der Vyver & Cowling (2019) were applied to field allometric measurements to produce AGC ground truth estimates for each of the 90 plots. These are shown against the WV3 2017 image in Figure 3.1.

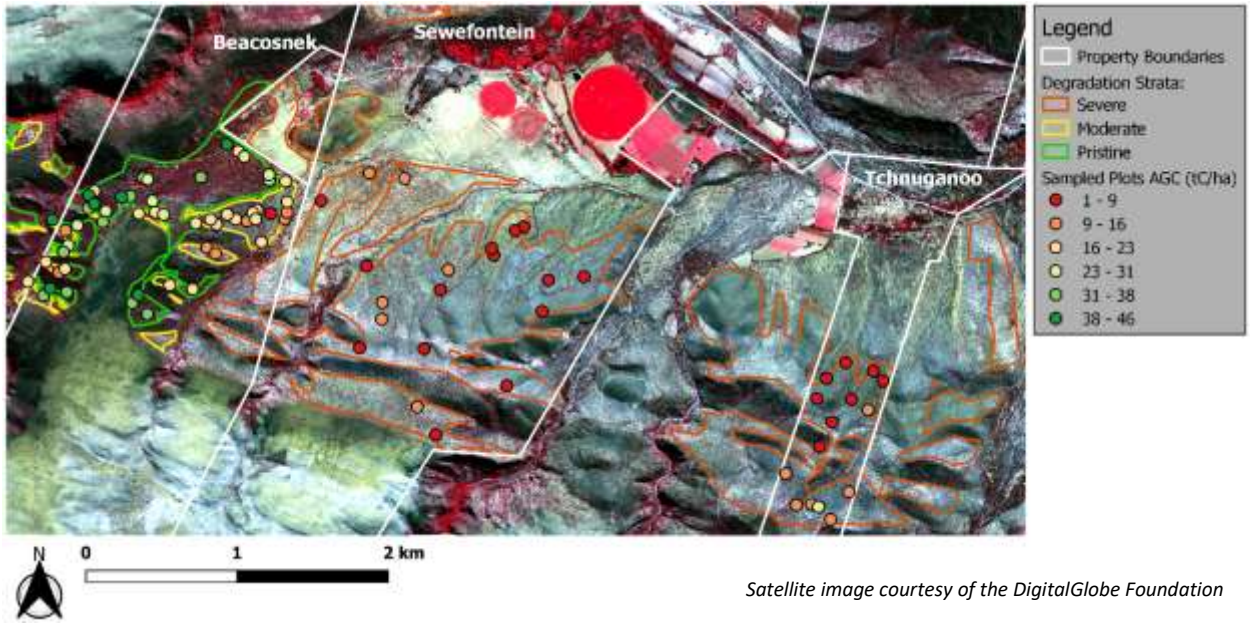


*Figure 3.1 AGC measurements against WorldView-3 background*

Figure 3.2 shows the change in AGC prediction accuracy ($R^2$ and negative RMSE) as successive features are added to the model with the stepwise forward selection procedure. The best multivariate model (in terms of both $R^2$ and RMSE) occurred with 24 features having been included. RMSE was evaluated using LOOCV, and $R^2$ found from the stacked predictions of the leave-one-out procedure.

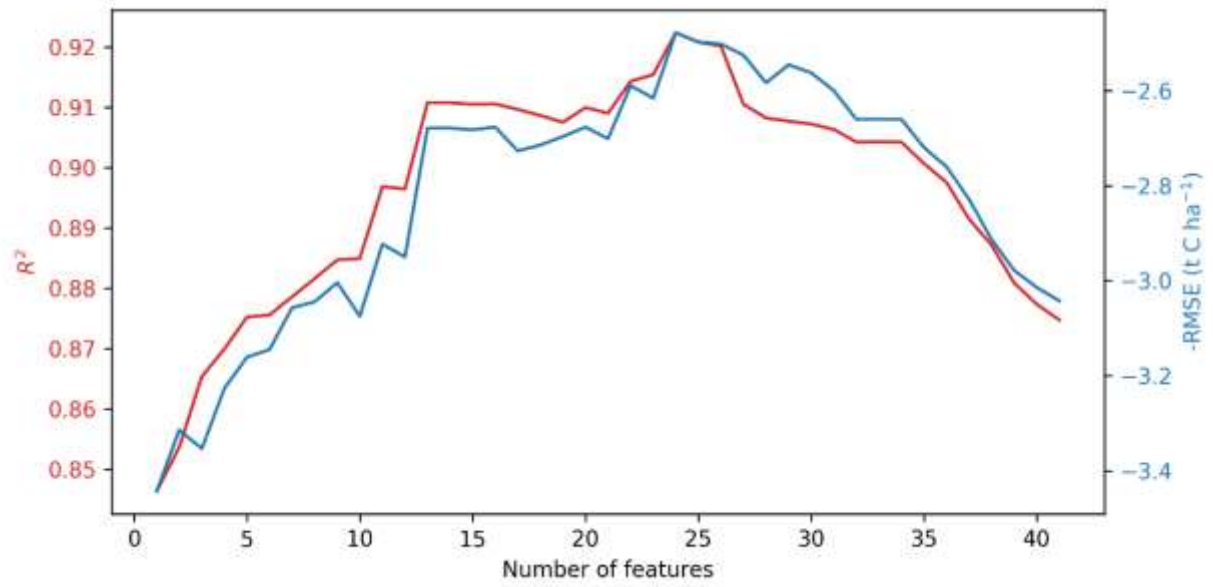


*Figure 3.2 Change in model accuracy with number of features*

The 24 features selected for best model are detailed in Table 3.1 (band symbols are defined in Table 2.3). The best univariate model uses the $Log(\overline{R/pan})$ feature (i.e. the first feature selected). Measured AGC is plotted against predicted AGC for the best multivariate and univariate models in Figure 3.3. Predicted AGC was again obtained from the LOOCV procedure.

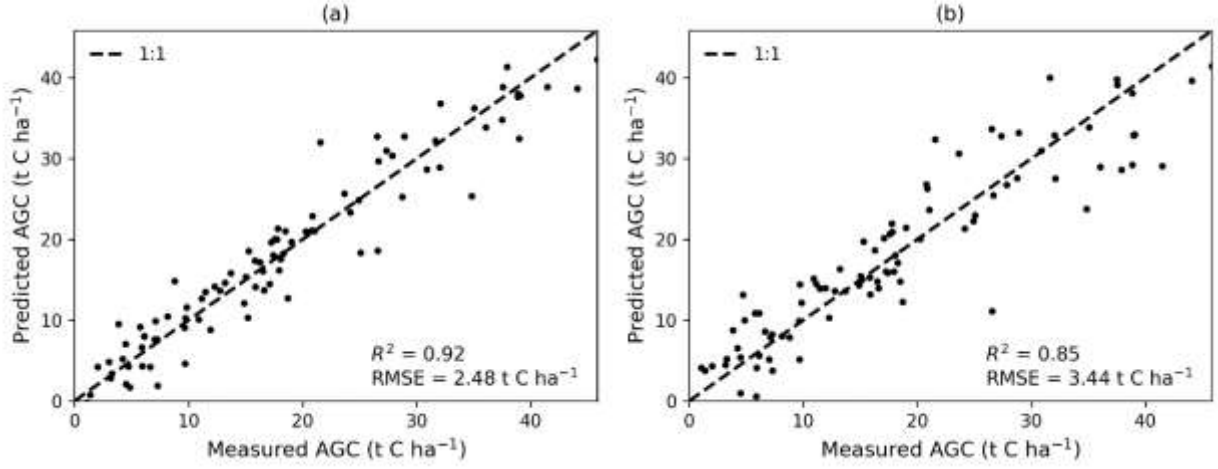


*Figure 3.3 Measured versus (a) multivariate, and (b) univariate, model predicted AGC*

*Table 3.1 Selected features*

| Rank | Feature | Coefficient |
|---|---|---|
| 1 | $Log(\overline{R/pan})$ | -254.5829 |
| 2 | $Std(pan/NIR2)$ | -178.3595 |
| 3 | $Std(C/R)$ | 91.2552 |
| 4 | $Log(\bar{B})$ | -18.1114 |
| 5 | $Std(C/RE)$ | 51.3412 |
| 6 | $Std(RE/NIR)$ | 10.7304 |
| 7 | $Entropy(NIR/Y)$ | -3.2045 |
| 8 | $Std(R/Y)$ | -0.7092 |
| 9 | $Std(C/Y)$ | 1.0605 |
| 10 | $(\overline{NIR/Y})^2$ | -0.2591 |
| 11 | $Std(B/C)$ | -54.2961 |
| 12 | $Entropy(G/C)$ | -5.6410 |
| 13 | $Entropy(SAVI_{NIR})$ | 1.4488 |
| 14 | $Entropy(RE/NIR2)$ | -2.2323 |
| 15 | $Std(B)$ | 0.0104 |
| 16 | $Entropy(B/NIR)$ | 7.4256 |
| 17 | $Entropy(Y/R)$ | 1.0666 |
| 18 | $Entropy(SAVI_{NIR2})$ | 4.6276 |
| 19 | $Std(NIR2/C)$ | 6.3905 |
| 20 | $Entropy(NIR2/Y)$ | 3.1364 |
| 21 | $Std(RE/R)$ | -10.1201 |
| 22 | $Entropy(pan/NIR)$ | -6.7159 |
| 23 | $Entropy(NIR2/C)$ | 2.4474 |
| 24 | $Entropy(RE/B)$ | -4.3346 |

Accuracies of the multivariate and univariate AGC models are compared in Table 3.2. RMSE confidence intervals are derived from the LOOCV RMSE values.

*Table 3.2 AGC regression evaluation (CI = confidence interval)*

| Description | Number of features | $R^2$ | RMSE (t C ha$^{-1}$) | 5-95% RMSE CI (t C ha$^{-1}$) |
|---|---|---|---|---|
| Multivariate | 24 | 0.9224 | 2.4781 | 0.2982 - 6.3566 |
| Univariate | 1 | 0.8464 | 3.4433 | 0.1705 - 9.4659 |

To better understand the influence of possibly noisy Litter C estimates on AGC, the correlation between litter C and ABC was examined, and is shown in Figure 3.4. Univariate and multivariate AGC maps derived from the WV3 2017 image are shown in Figure 3.5.

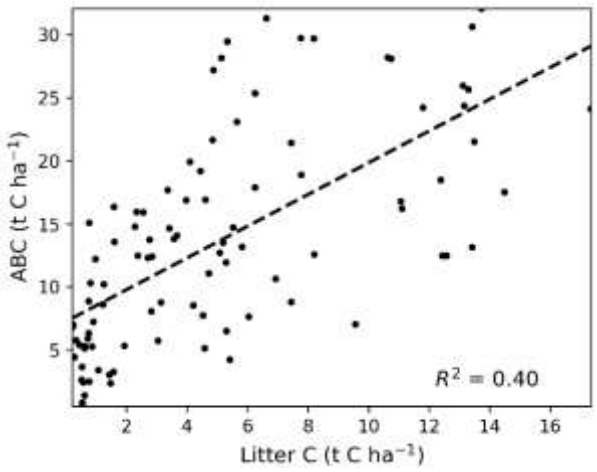


*Figure 3.4 Litter C and ABC correlation*

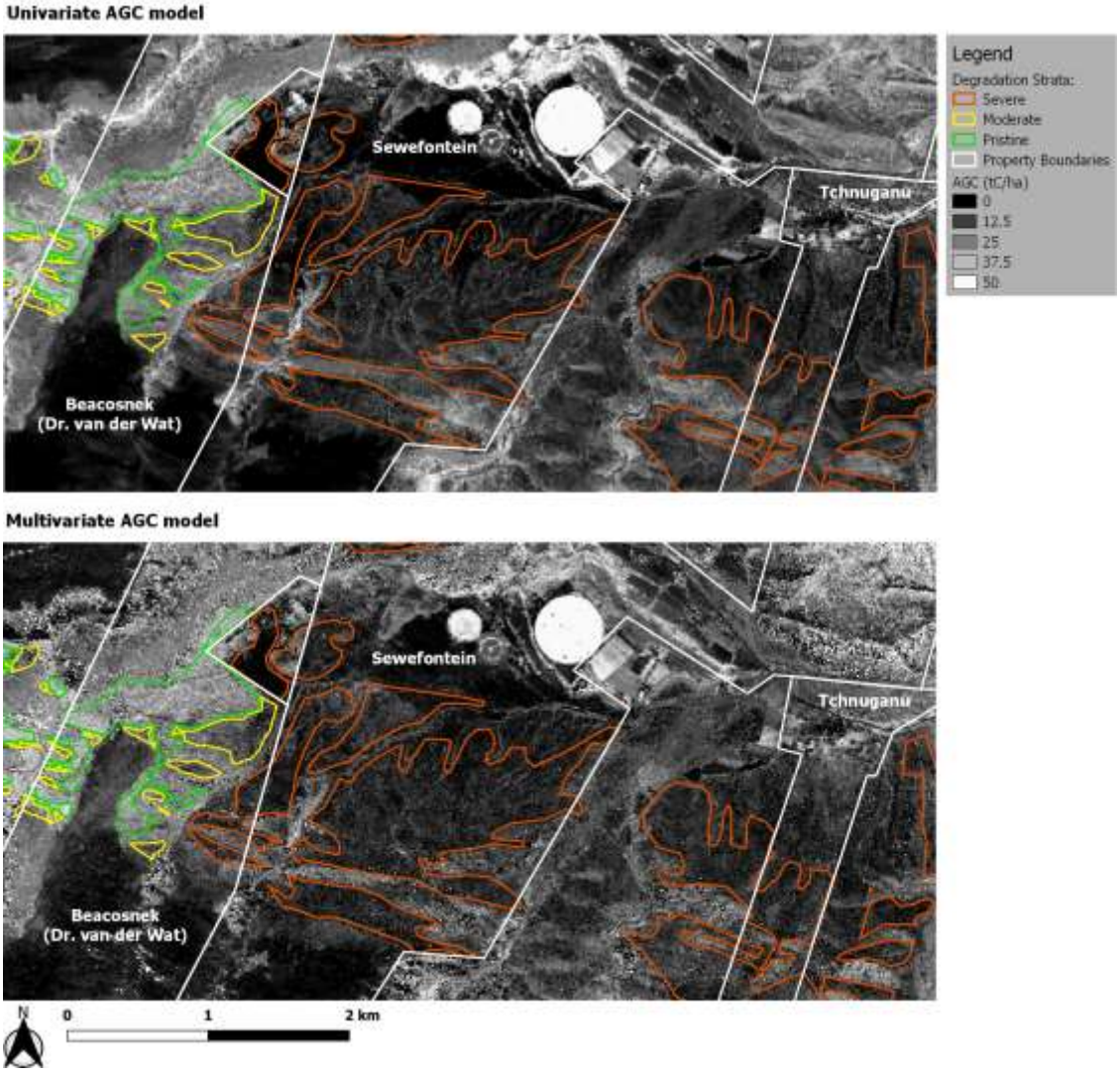


*Figure 3.5 Univariate and multivariate AGC maps of the study area*

## 3.2 Temporal transferability

Table 3.3 gives an indication of the suitability of selected features for temporal calibration, where the final column serves as an overall suitability score. Table 3.4 and Table 3.5 show the mean of the calibrated AGC model $R^2$ and RMSE values respectively, over 20 bootstraps of each *model* - *calibration* image combination. *Model* images are listed down the columns and *calibration* images along the rows.

*Table 3.3 Feature transferability and relevance.*

| Feature | [a] WV3 2017 AGC Model $R^2$ | [b] WV3 2017 - WV3 2018 $R^2$ | [c] WV3 2017 - NGI 2015 $R^2$ | [d] Mean $R^2$ |
|---|---|---|---|---|
| $Log(\overline{R/pan})$ | 0.8404 | 0.9704 | 0.9090 | 0.9066 |
| $Log(\overline{G/R})$ | 0.7993 | 0.9760 | 0.9164 | 0.8972 |
| $Log(\overline{R/NIR})$ | 0.7848 | 0.9420 | 0.8842 | 0.8703 |
| $NDVI$ | 0.7704 | 0.9400 | 0.8777 | 0.8627 |
| $SAVI$ | 0.7704 | 0.9400 | 0.8777 | 0.8627 |
| $Log(\overline{B/R})$ | 0.7488 | 0.9808 | 0.8236 | 0.8511 |

[a] the accuracy of a univariate model on the WV3 2017 image, [b] correlation between WV3 2017 and WV3 2018 images, [c] correlation between WV3 2017 and NGI 2015 images, [d] mean of the previous three columns

*Table 3.4 Mean AGC $R^2$ values for temporal calibration between images*

| | | Calibration images | | |
|---|---|---|---|---|
| | | **WV3 2017** | **WV3 2018** | **NGI 2015** |
| **Model images** | **WV3 2017** | | 0.8306 | 0.7253 |
| | **WV3 2018** | 0.8428 | | 0.7294 |
| | **NGI 2015** | 0.8152 | 0.8051 | |

*Table 3.5 Mean AGC RMSE (t C $ha^{-1}$) values for calibration between images*

| | | Calibration images | | |
|---|---|---|---|---|
| | | **WV3 2017** | **WV3 2018** | **NGI 2015** |
| **Model images** | **WV3 2017** | | 4.7639 | 6.0685 |
| | **WV3 2018** | 4.5940 | | 6.0273 |
| | **NGI 2015** | 4.9659 | 5.0973 | |

## 3.3 AGC from plant volume

The correlation of ABC and AGC with biomass volume is shown in Figure 3.6. Table 3.6 shows the LOOCV $R^2$ and RMSE accuracies and confidence intervals for linear models predicting ABC and AGC from biomass volume.

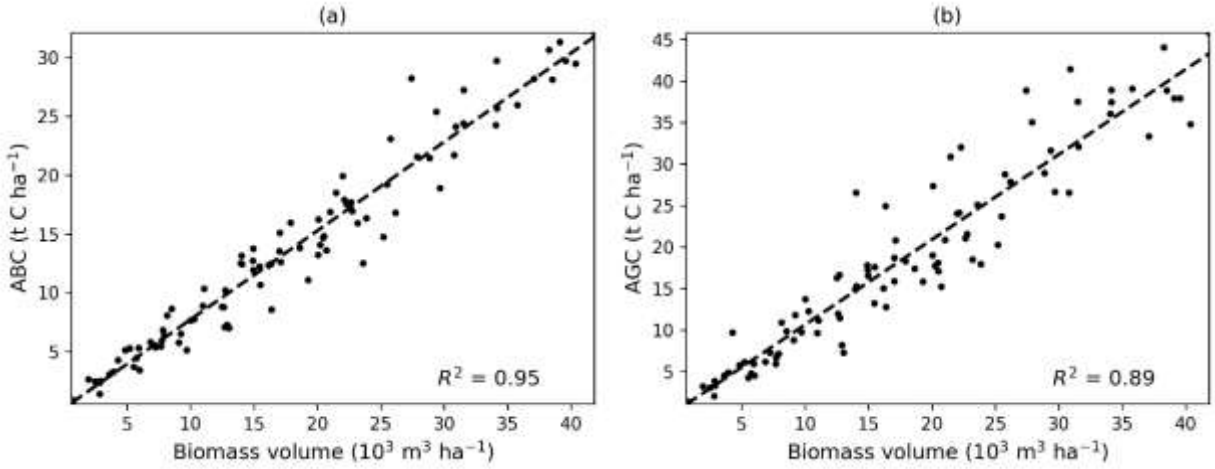


*Figure 3.6 Predicting (a) ABC, and (b) AGC from biomass volume*

*Table 3.6 Accuracy of predicting ABC/AGC from biomass volume (CI = confidence interval)*

| Model | $R^2$ | RMSE (t C ha$^{-1}$) | 5-95% RMSE CI (t C ha$^{-1}$) |
|---|---|---|---|
| ABC | 0.9462 | 1.3947 | 0.0608 - 3.8265 |
| AGC | 0.8928 | 2.8206 | 0.3660 - 8.1040 |

As an illustration of the potential of deriving vegetation height from VHSR DSMs, a 3D rendering of the DSM draped with the WV3 2017 image is shown in Figure 3.7.

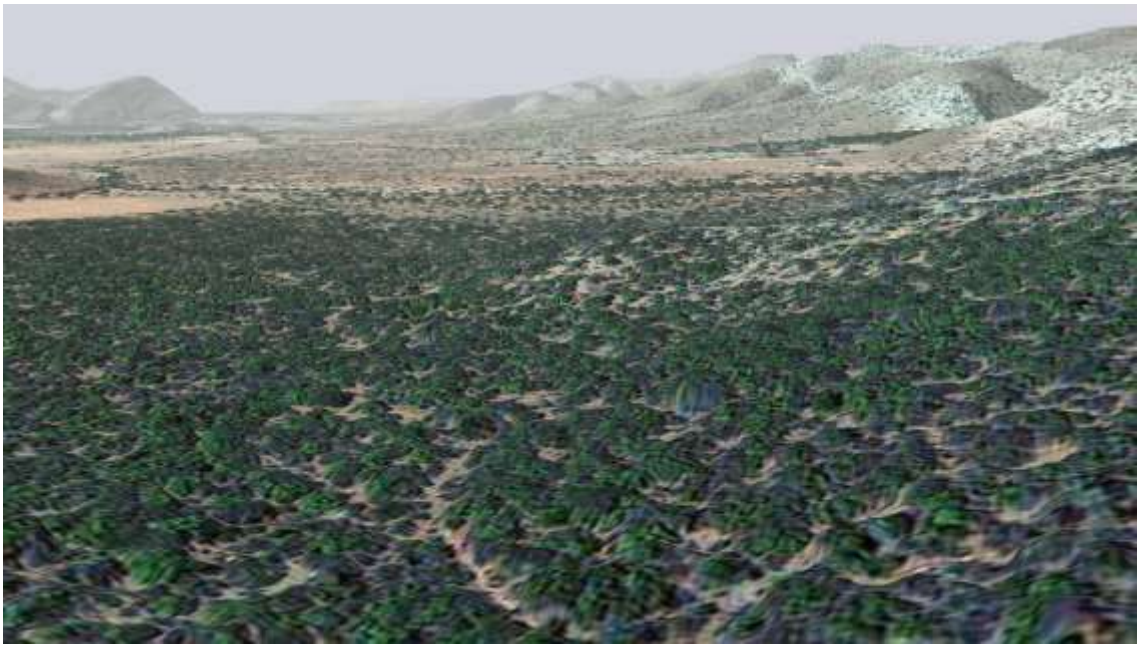

*Figure 3.7 3D rendering of study area (WorldView-3 imagery draped on NGI DSM)*

# 4 Discussion

## 4.1 Snapshot AGC regression model

Figure 3.2 shows typical effects of increasing complexity on model accuracy. As the number of features increases from one to 24, the explanatory power of the model increases with an associated increase in accuracy. With more than 24 features, overfitting begins to occur as there insufficient data to represent the underlying dimensionality. This is known as the "peaking phenomenon" and is the main motivation for feature selection (Jain, Duin & Mao 2000).

Selected features (Table 3.1) include a combination of band ratio and texture features (and non-linear transformations thereof). Band ratios describe spectral properties of vegetation, such as greenness or relative shape of the red-edge. In remote sensing of biomass, texture features are known to complement spectral information (Lu et al. 2016; Lu 2006). A number of entropy and standard deviation features are also included in the selected set, confirming the usefulness of texture for predicting AGC. Note that grey-level co-occurrence matrix (GLCM) texture features (Haralick, Shanmugam & Dinstein 1973) were also tested, but did not improve on the simple standard deviation and entropy descriptors.

Multivariate and univariate linear regression model accuracies are reported in Table 3.2. The performance of the multivariate model ($R^2$ = 0.92 and RMSE = 2.48 t C $ha^{-1}$) compares well with related studies (Ali et al. 2015; Eisfelder, Kuenzer & Dech 2012) and would be useful for operational AGC estimation. Non-parametric support vector regression (SVR) models were also evaluated, but did not improve on the accuracy of the multivariate linear model with stepwise forward selection. As it stands, the remote sensing approach is valid for inclusion under the AR-ACM0003 CDM methodology (CDM 2013), preferred for restoration projects in thicket, and consequently provides an opportunity to reduce the monitoring costs for this and other restoration carbon projects in the thicket biome.

AGC maps produced by applying the univariate and multivariate AGC models to the WV3 2017 image are shown in Figure 3.5. As the sampling plots were all located in thicket habitat, the AGC values for other vegetation may not be valid. The multivariate AGC output is slightly noisy in some thicket areas. This is due to the inclusion of texture features in the multivariate model which are sensitive to sudden changes in illumination caused by e.g. shadows and sun-glint off bare rock. In practice, these effects will be averaged out when aggregating AGC values over extended areas.

It is known that biomass estimation accuracy is sensitive to sampling plot size and positional accuracy (Frazer et al. 2011; Réjou-Méchain et al. 2019). Given the relatively small sampling plots used in this study (see e.g. Frazer et al. (2011) for commonly used plot sizes), a strong emphasis was placed on achieving sub-meter spatial accuracy of image orthorectification and recorded plot location. This allowed precise location of sampling plots in the image and contributed to the success of the method.

The high correlation between field measured and model predicted AGC supports the use of the adopted sampling protocol ("standard operating procedure" (SOP)) (Bolus et al. 2018) for generating meaningful remote sensing ground truth data. The nesting approach (Lackmann 2011) used in the SOP substantially reduces the number of plants requiring measurement with a negligible impact on AGC estimation accuracy. Nested plot size and plant height thresholds were chosen conservatively based on an analysis of limited trial data (Appendix A) to ensure accurate AGC estimation. It is recommended that the complete set of sampling data be analysed to investigate further optimisations to the sampling protocol. Small adjustments to the nesting approach can have a large impact on the cost of field work, which is currently a limiting factor in scaling up restoration (Powell 2009; Van der Vyver & Cowling 2019).

The litter sampling approach is another aspect of the SOP that could benefit from further investigation, and possible modification. Litter C forms a substantial component of AGC in intact subtropical thicket (e.g. the average the ratio of Litter C to ABC was 0.48 for the intact stratum), and it is known that litter C forms a greater component of AGC in subtropical thicket than in other habitats (Lechmere-Oertel et al. 2008). Given the importance of litter C in thicket, one should ensure it is sampled accurately. It is questionable, however, if litter C sampled from four 0.5 m x 0.5 m plots is representative of litter C in the much larger containing plot. The combined area of the litter sample is 1 $m^2$, while the containing plot area is 100 $m^2$ or 400 $m^2$, depending on the stratum. Intuitively, it seems likely that in heterogeneous thicket habitats the small area litter sample will be noisy relative to what is contained in the larger plot. This hypothesis would help explain the weak correlation ($R^2$ = 0.40) between Litter C and ABC shown in Figure 3.4. A simple means of improving litter C accuracy would be to increase the litter C plot size(s), but this comes at the cost of increased field work. Alternatively one could use a per-stratum litter C value (as per Equation 13 in CDM (2015)) calculated from the average of all litter samples in the stratum. This could help average out noisy per-plot estimates and improve the accuracy of remotely sensed AGC.

## 4.2 Temporal transferability

As a first indication of model temporal transferability, correlation of sampling plot image features between the WV3 2017 - WV3 2018 and WV3 2017 - NGI 2015 images are reported in in the "WV3 2017 - WV3 2018 $R^2$" and "WV3 2017 – NGI 2015 $R^2$" columns in Table 3.3. The $Log(\overline{R/pan})$ and $Log(\overline{G/R})$ features are both strongly correlated between images, indicating that they remain relatively consistent over time and are insensitive to radiometric (atmospheric and anisotropic) variations, i.e. these features are well suited to temporal calibration. The usefulness of these features for predicting AGC is indicated

by values in "WV3 2017 AGC Model $R^2$" column in Table 3.3. Somewhat fortuitously, both features are well correlated with AGC, with the $Log(\overline{R/pan})$ feature being the best single feature for AGC prediction (i.e. the feature used in the univariate AGC model). Overall suitability of features (in terms of strength of correlation with AGC and consistency over time) is measured as the mean of the three $R^2$ values ("WV3 2017 AGC Model $R^2$", "WV3 2017 - WV3 2018 $R^2$" and "WV3 2017 – NGI 2015 $R^2$") for each feature and reported in the "Mean $R^2$" column in Table 3.3. According to this analysis, $Log(\overline{R/pan})$ is the top ranked feature and was therefore used for univariate AGC modelling in the temporal calibration experiments. LOOCV performance of the $Log(\overline{R/pan})$ model on the WV3 2017 image is reported in Table 3.2.

$R^2$ and RMSE performance of the calibrated AGC models is given in Table 3.4 and Table 3.5 respectively. Performance is good on the whole and suggests the temporal calibration approach is sufficient for repeated images of the same area. As temporal calibration acts as an additional source of error, performance of the calibrated univariate models is slightly worse than that of snapshot univariate model (Table 3.2), but not significantly so. The accuracies involving the NGI 2015 as image (either as *model* or *calibration* image, but especially as *calibration* image) are relatively worse than those involving only WorldView-3 images. This is not particularly surprising given the large time gap between the NGI image and time of field sampling, in addition to spectral and spatial resolution differences between the WordView-3 and NGI sensors. Nevertheless, it is useful to know that NGI aerial imagery can also provide good AGC prediction accuracy. This is relevant to biome-wide AGC mapping where cost and coverage of the NGI imagery will be advantages over commercial satellite imagery.

The temporal calibration experiments discussed here were an initial investigation based on available data. Some aspects of the approach deserve further attention. Additional experiments are recommended to investigate criteria for selection of appropriate invariant calibration sites. The possibility of extending calibration to multivariate models should also be researched, in combination with a broader study to identify suitable features for use in such models. A comprehensive validation of the technique should involve longer time periods between images with repeat AGC field sampling.

## 4.3 AGC from plant volume

The estimated plant volumes are strongly correlated with ABC and AGC ($R^2$ = 0.95 and $R^2$ = 0.89 respectively), as can be seen in Figure 3.6. This is an important result, as it implies that if a reliable means for remote sensing of plant volume can be devised, it would be an effective predictor of ABC. Aerial LIDAR surveys are frequently used in similar applications to measure plant volume, but are costly and present problems in dense short stature habitats (Kulawardhana, Popescu & Feagin 2017). Alternatively, high resolution DSMs can be derived from stereo aerial imagery using photogrammetry. Plant height information can conceivably be derived from this form of DSM (see Figure 3.7). The latest 0.25 m resolution, national coverage imagery being captured by NGI is free of charge and well-suited to this approach. Unmanned aerial vehicles (UAVs) are another option for building DSMs (Matese, Di Gennaro & Berton 2017), albeit of small areas. The use of photogrammetry for measuring vegetation volume is, however, a new field with very little research (Lu et al. 2016).

Multi-spectral (radiometric) approaches to biomass estimation suffer from sensitivity to variations in atmospheric conditions, anisotropy and phenology which inhibit their transferability over space and time (Eisfelder, Kuenzer & Dech 2012; Lu et al. 2016). The volume (geometric) approach is appealing due to its simplicity and lack of sensitivity to these sources of variation. It is not without its own difficulties, however. With photogrammetry, the extraction of ground height from the DSM is a major challenge in

densely vegetated habitats, such as subtropical thicket. Currently, there is no reliable method for addressing this crucial component of the volume approach (Gillan et al. 2014; Matese, Di Gennaro & Berton 2017). Due to the uncertainties surrounding the volume approach, the multi-spectral method presented in this report is the recommended approach for AGC mapping in thicket at present.

## 4.4 Practical application and future work

AGC maps of the study area, derived from the WV3 2017 image, are shown in Figure 3.5. These serve as a baseline carbon assessment for future restoration or other studies in the area. Estimated accuracies of the AGC models are given in Table 3.2.

For repeat AGC maps of the study area, the univariate AGC model can be calibrated and applied to new WorldView-3 (or similar) images as described in section 2.4. New images should ideally be captured at a similar time of year to the WV3 2017 image (i.e. October) to reduce phenological variation. Example accuracies for the temporal calibration are given in section 3.2 and discussed in section 4.2. Given the limitations of the temporal calibration experiments discussed in section 4.2, it would be helpful if repeat applications are accompanied by reduced field sampling exercises (± 10 plots spread over the thicket degradation strata) to validate accuracy of the repeat map. Repeat maps would be useful for monitoring AGC changes over time, and could be used for carbon accreditation.

Spatial extension of the method to new areas has not been tested. Intuitively, it seems likely that the structure and features of simple AGC models, such as those used in the temporal calibration, will remain valid for new areas, but will require a new parameterisation to account for habitat and radiometric variation. Initially, this concept should be validated with comprehensive field sampling similar to that undertaken for the GEF5 SLM project. Once confidence in the methodology is established, extension to new areas could conceivably be achieved with substantially reduced (± 10 plot) sampling exercises, that would be used to calibrate the model to local conditions.

Two-step or multi-scale approaches are seeing increasing use for regional or national scale vegetation mapping (González-Roglich & Swenson 2016; Immitzer et al. 2018; Mathieu et al. 2018). In these approaches, small scale field ground truth is extrapolated to larger spatial extents using regression modelling with VHSR imagery. In a second step, medium resolution imagery (such as Landsat or Sentinel) is used with the extrapolated ground truth to derive vegetation maps over much larger spatial extents. The multi-scale approach achieves a good compromise between the costs and benefits of the field, VHSR and medium resolution worlds, and represents a promising avenue for biome-wide AGC mapping in thicket.

# 5 Conclusion

A snapshot regression model using 24 band ratio, vegetation index and textural features from WorldView-3 imagery provided good AGC prediction accuracy ($R^2$ = 0.92 and RMSE = 2.48 t C $ha^{-1}$). To facilitate the repeat generation of AGC maps, a temporal calibration method was devised and evaluated on a set of three images. The method uses a linear transform fitted to invariant plots to calibrate appropriate image features for use in a univariate AGC model. Overall $R^2$ and RMSE performance of the calibrated models was 0.79 and 5.25 t C $ha^{-1}$ respectively, demonstrating the potential of the method to address the challenge of temporal transferability. Spatial extension of the AGC model to new areas should be tested with the acquisition of further imagery and ground truth. While remote sensing of plant volume with LiDAR or stereo aerial imagery could prove to be effective for mapping thicket AGC,

challenges with those approaches precluded their evaluation in this study. The results of this, and the Nyamugama & Kakembo (2015) study, demonstrate the efficacy of multi-spectral imagery for accurate remote sensing of AGC in thicket. AGC maps will assist in the planning and monitoring of restoration, verification of stored carbon and understanding of thicket ecosystem dynamics. The presented remote sensing approach qualifies for inclusion under the AR-ACM0003 CDM methodology (CDM 2013), preferred for thicket restoration projects, and consequently provides an opportunity to reduce the monitoring costs for this and other restoration carbon projects in the thicket biome.

## Acknowledgements

The WV3 2017 image was acquired courtesy of the DigitalGlobe Foundation (DigitalGlobe 2019). Adriaan van Niekerk and the Centre for Geographical Analysis (CGA) at Stellenbosch University assisted with the acquisition of the WV3 2018 and NGI 2015 imagery, and provision of software for orthorectification and atmospheric correction. The authors thank Mike and Rebecca Powell for ongoing discussions that helped shape and direct this study. DGPS devices for field work were obtained on loan from the Departments of Geography at Stellenbosch and Rhodes Universities. Melloson Allen from Living Lands, and Hanton Windvogel assisted with field work.

# References

Agisoft 2019. Agisoft Metashape [online]. Available from: https://www.agisoft.com/ [Accessed 30 October 2019].

Ali I, Greifeneder F, Stamenkovic J, Neumann M & Notarnicola C 2015. Review of machine learning approaches for biomass and soil moisture retrievals from remote sensing data. *Remote Sensing* 7, 12: 16398-16421.

Bayer AD, Bachmann M, Rogge D, Muller A & Kaufmann H 2016. Combining field and imaging spectroscopy to map soil organic carbon in a semiarid environment. *IEEE Journal of Selected Topics in Applied Earth Observations and Remote Sensing* 9, 9: 3997-4010.

Bishop CM 2003. *Neural networks for pattern recognition*. New York: Oxford University Press.

Blauensteiner P, Wildenauer H, Hanbury A & Kampel M 2006. *On colour spaces for change detection and shadow suppression*. Proceedings of Computer Vision Winter Workshop 2006. Telc: 1-6.

Bolus C, Harris D, Reeler J, Powell MJ, Powell RL & Ngwenya M 2020. *Above ground carbon baseline assessment, using species specific allometric models, across three degradation classes in Baviaanskloof Spekboom Thicket*. Makhanda: GEF5 SLM.

Bolus C, Reeler J, Harris D, Powell MJ & Powell RL 2018. *Standard operating procedure (SOP) for above ground carbon baseline field sampling*. v.01. Cape Town: GEF5 SLM PROJECT.

Campbell JB & Wynne RH 2011. *Introduction to remote sensing*. New York: The Guilford Press.

CDM 2013. *A/R Large-scale consolidated methodology: Afforestation and reforestation of lands except wetlands*. 2.

CDM 2015. *A/R Methodological tool: Estimation of carbon stocks and change in carbon stocks in dead wood and litter in A/R CDM project activities*.

Clarke C, Shackleton S & Powell M 2012. Climate change perceptions, drought responses and views on carbon farming amongst commercial livestock and game farmers in the semiarid Great Fish River Valley, Eastern Cape province, South Africa. *African Journal of Range & Forage Science* 29: 13-23.

Cowling RM, ProcheÕ Ô & Vlok JHJ 2005. On the origin of southern African subtropical thicket vegetation. *South African Journal of Botany* 71, 1: 1-23.

DigitalGlobe 2019. DigitalGlobe Foundation [online]. Available from: http://foundation.digitalglobe.com/ [Accessed 1 November 2019].

Eisfelder C, Kuenzer C & Dech S 2012. Derivation of biomass information for semi-arid areas using remote-sensing data. *International Journal of Remote Sensing* 33, 9: 2937-2984.

ESA 2007. TerraSAR-X [online]. Available from: https://spacedata.copernicus.eu/web/cscda/missions/terrasar-x [Accessed 26 October 2019].

Fassnacht FE, Hartig F, Latifi H, Berger C, Hernández J, Corvalán P & Koch B 2014. Importance of sample size, data type and prediction method for remote sensing-based estimations of aboveground forest biomass. *Remote Sensing of Environment* 154, 1: 102-114.

Fassnacht FE, Latifi H, Stereńczak K, Modzelewska A, Lefsky M, Waser LT, Straub C & Ghosh A 2016. Review of studies on tree species classification from remotely sensed data. *Remote Sensing of*

*Environment* 186: 64-87.

Frazer GW, Magnussen S, Wulder MA & Niemann KO 2011. Simulated impact of sample plot size and co-registration error on the accuracy and uncertainty of LiDAR-derived estimates of forest stand biomass. *Remote Sensing of Environment* 115, 2: 636-649.

GEF 2013. Securing multiple ecosystems benefit through SLM in the productive but degraded landscapes of South Africa [online]. Available from: https://www.za.undp.org/content/south_africa/en/home/operations/projects/environment_and_energy/the-gef-small-grant-programme-.html [Accessed 27 October 2019].

Gillan JK, Karl JW, Duniway M & Elaksher A 2014. Modeling vegetation heights from high resolution stereo aerial photography: An application for broad-scale rangeland monitoring. *Journal of Environmental Management* 144, June: 226-235.

Goetz SJ, Baccini A, Laporte NT, Johns T, Walker W, Kellndorfer J, Houghton RA & Sun M 2009. Mapping and monitoring carbon stocks with satellite observations: a comparison of methods. *Carbon Balance and Management* 4, 2: 1-7.

González-Roglich M & Swenson JJ 2016. Tree cover and carbon mapping of Argentine savannas: Scaling from field to region. *Remote Sensing of Environment* 172: 139-147.

Haralick RM, Shanmugam K & Dinstein I 1973. Textural features for image classification. *IEEE Transactions on Systems, Man, and Cybernetics* SMC-3, 6: 610-621.

Harris D & Van Niekerk A 2018. Feature clustering and ranking for selecting stable features from high dimensional remotely sensed data. *International Journal of Remote Sensing* 39, 23: 8934-8949.

Harris D & Van Niekerk A 2019. Radiometric homogenisation of aerial images by calibrating with satellite data. *International Journal of Remote Sensing* 40, 7: 2623-2647.

Harris D, Vlok J & Van Niekerk A 2018. Regional mapping of spekboom canopy cover using very high resolution aerial imagery. *Journal of Applied Remote Sensing* 12, 04: 1.

Hoare DB, Mucina L, Rutherford MC, Volk JHJ, Euston-Brown DIW, Palmer AR, Powrie LW, Lechmere-Oertel RG, Proches SM, Dold AP & Ward RA 2006. Albany Thicket Biome. *The vegetation of South Africa, Lesotho and Swaziland* , Strelitzia 19: 541-567.

Huete AR 1988. A soil-adjusted vegetation index (SAVI). *Remote Sensing of Environment* 25, 3: 295-309.

Immitzer M, Böck S, Einzmann K, Vuolo F, Pinnel N, Wallner A & Atzberger C 2018. Fractional cover mapping of spruce and pine at 1 ha resolution combining very high and medium spatial resolution satellite imagery. *Remote Sensing of Environment* 204: 690-703.

Jain AK, Duin RPW & Mao J 2000. Statistical pattern recognition: A review. *IEEE Transactions on Pattern Analysis and Machine Intelligence* 22, 1: 4-37.

Kulawardhana RW, Popescu SC & Feagin RA 2017. Airborne lidar remote sensing applications in non-forested short stature environments: A review. *Annals of Forest Research* 60, 1: 127-150.

Lackmann S 2011. Good practice in designing a forest inventory. *Coalition for Rainforest Nations* , May: 75.

Lechmere-Oertel RG, Kerley GIH & Cowling RM 2005. Patterns and implications of transformation in

semi-arid succulent thicket, South Africa. *Journal of Arid Environments* 62, 3: 459-474.

Lechmere-Oertel RG, Kerley GIH, Mills AJ & Cowling RM 2008. Litter dynamics across browsing-induced fenceline contrasts in succulent thicket, South Africa. *South African Journal of Botany* 74, 4: 651-659.

Lloyd JW, Van den Berg EC & Palmer AR 2002. *Patterns of transformation and degradation in the Thicket Biome, South Africa*. Publication No GW/A/2002/30. Port Elizabeth: Terrestrial Ecology Research Unit, University of Port Elizabeth.

Lu D 2006. The potential and challenge of remote sensing-based biomass estimation. *International Journal of Remote Sensing* 27, 7: 1297-1328.

Lu D, Chen Q, Wang G, Liu L, Li G & Moran E 2016. A survey of remote sensing-based aboveground biomass estimation methods in forest ecosystems. *International Journal of Digital Earth* 9, 1: 63-105.

Marais C, Cowling RM & Powell M 2009. *Establishing the platform for a carbon sequestration market in South Africa: The Working for Woodlands Subtropical Thicket Restoration Programme*. Proceedings of XIII World Forestry Congress. Buenos Aires: 1-13.

Matese A, Di Gennaro SF & Berton A 2017. Assessment of a canopy height model (CHM) in a vineyard using UAV-based multispectral imaging. *International Journal of Remote Sensing* 38, 8-10: 2150-2160.

Mather PM & Koch M 2011. *Computer processing of remotely-sensed images*. Chichester: John Wiley & Sons.

Mathieu R, Wessels K, Main R, Naidoo L, van der Bergh F & Erasmus B 2018. A radar- and LiDAR-based earth observation system for monitoring savanna woody structure in southern Africa. *Biodiversity & Ecology* 6: 355-359.

Mills AJ, Blignaut J, Cowling RM, Knipe A, Marais C, Marais S, Pierce S, Powell M, Sigwela A & Skowno A 2010. *Investing in sustainability. Restoring degraded thicket, creating jobs, capturing carbon and earning green credit*. Port Elizabeth: Climate Action Partnership, Cape Town and Wilderness Foundation.

Mills AJ & Cowling RM 2006. Rate of carbon sequestration at two thicket restoration sites in the Eastern Cape, South Africa. *Restoration Ecology* 14, 1: 38-49.

Mills AJ & Cowling RM 2014. How fast can carbon be sequestered when restoring degraded subtropical thicket? *Restoration Ecology* 22, 5: 571-573.

Mills AJ, Cowling RM, Fey M, Kerley G, Donaldson J, Sigwela A, Skowno A & Rundel P 2005. Effects of goat pastoralism on ecosystem carbon storage in semiarid thicket, Eastern Cape, South Africa. *Austral Ecology* 30: 797-804.

Mills AJ, Turpie JK, Cowling RM, Marais C, Kerley G, Richard G, Sigwela A & Powell M 2007. Assessing costs, benefits, and feasibility of restoring natural capital in Subtropical Thicket in South Africa. In Aronson J, Milton S & Blignaut J (eds) *Restoring Natural Capital: Science, Business and Practice (The Science and Practice of Ecological Restoration Series)*, 179-187. Washington DC: Island Press.

Mills AJ, Van der Vyver M, Gordon IJ, Patwardhan A, Marais C, Blignaut J, Sigwela A & Kgope B 2015.

Prescribing innovation within a large-scale restoration programme in degraded subtropical thicket in South Africa. *Forests* 6, 11: 4328-4348.

National Geo-spatial Information 2012. National aerial photography and imagery programme [online]. Available from: http://www.ngi.gov.za/index.php/what-we-do/aerial-photography-and-imagery [Accessed 22 May 2012].

Nyamugama A & Kakembo V 2015. Estimation and monitoring of aboveground carbon stocks using spatial technology. *South African Journal of Science* 111, 9-10: 1-7.

Powell MJ 2009. Restoration of degraded subtropical thickets in the Baviaanskloof Megareserve, South Africa. Master's Thesis. Grahamstown: Rhodes University, Department of Environmental Science.

Powell MJ, Mills AJ & Marais C 2005. Carbon sequestration and restoration: Challenges and opportunities in subtropical thicket [online]. Available from: https://www.daff.gov.za/daffweb3/Portals/0/General Reports/4271___Day2_session3_item1.pdf [Accessed 29 December 2018].

Réjou-Méchain M, Barbier N, Couteron P, Ploton P, Vincent G, Herold M, Mermoz S, Saatchi S, Chave J, de Boissieu F, Féret J-B, Takoudjou SM & Pélissier R 2019. Upscaling forest biomass from field to satellite measurements: Sources of errors and ways to reduce them. *Surveys in Geophysics* 40, 4: 881-911.

Richter R 1997. Correction of atmospheric and topographic effects for high spatial resolution satellite imagery. *International Journal of Remote Sensing* 18, 5: 1099-1111.

Sigwela A, Kerley G, Mills AJ & Cowling RM 2009. The impact of browsing-induced degradation on the reproduction of subtropical thicket canopy shrubs and trees. *South African Journal of Botany* 75, 2: 262-267.

Skowno A & Euston-Brown DIW 2006. BMR Vegetation 2006 [online]. Available from: http://bgis.sanbi.org/SpatialDataset/Detail/249 [Accessed 30 October 2019].

Thompson M, Vlok JHJ, Rouget M, Hoffman MT & Cowling RM 2009. Mapping grazing-induced degradation in a semi-arid environment: A rapid and cost-effective approach for assessment and monitoring. *Environmental Management* 43: 585-596.

Trias-Sanz R, Stamon G & Louchet J 2008. Using colour, texture, and hierarchial segmentation for high-resolution remote sensing. *ISPRS Journal of Photogrammetry and Remote Sensing* 63, 2: 156-168.

Vlok JHJ 2017. *Guidelines for spekboom and veld restoration on sewefontein and tchuganoo*.

Vlok JHJ, Cowling RM & Wolf T 2005. *A vegetation map for the Little Karoo*. Unpublished maps and report for a SKEP project supported by CEPF grant no 1064410304.

Vlok JHJ & Euston-Brown DIW 2002. *The patterns within, and the ecological processes that sustain, the subtropical thicket vegetation in the planning domain of the Subtropical Thicket Ecosystem Planning (STEP) project*. Publication No 40. Port Elizabeth: Terrestrial Ecology Research Unit, University of Port Elizabeth.

Van der Vyver ML 2017. Factors affecting effective ecological restoration of Portulacaria afra (spekboom)-rich subtropical thicket and aboveground carbon end- point projections. Nelson Mandela University.

Van der Vyver ML 2017. Thicket allometric models. Nelson Mandela University.

Van der Vyver ML & Cowling RM 2019. Aboveground biomass and carbon pool estimates of Portulacaria afra (spekboom)-rich subtropical thicket with species-specific allometric models. *Forest Ecology and Management* 448: 11-21.

Van der Vyver ML, Cowling RM, Mills AJ & Difford M 2013. Spontaneous return of biodiversity in restored subtropical thicket: *Portulacaria afra* as an ecosystem engineer. *Restoration Ecology* 21, 6: 736-744.

# Appendix A Trial data analysis for carbon sampling methodology design

This document presents the results of a data analysis exercise conducted on the GEF 2017 field trial data. As part of the trial, allometry was conducted for all plant species in five plots. Two plots were located in degraded thicket and three in intact thicket. Allometric models for thicket species were obtained from Marius van der Vyver (M.L. Van der Vyver 2017). Where there were measurement records for species that hadn't yet been identified, an allometric model for what is assumed to be a similar species was used. E.g. for "Asparagus hairy", the "Asparagus capensis" model was used. No obvious species choice could be made for some of these unidentified measurement records. The records for these cases formed a small portion of the total and were omitted from the analysis.

## A.1 Woody Canopy

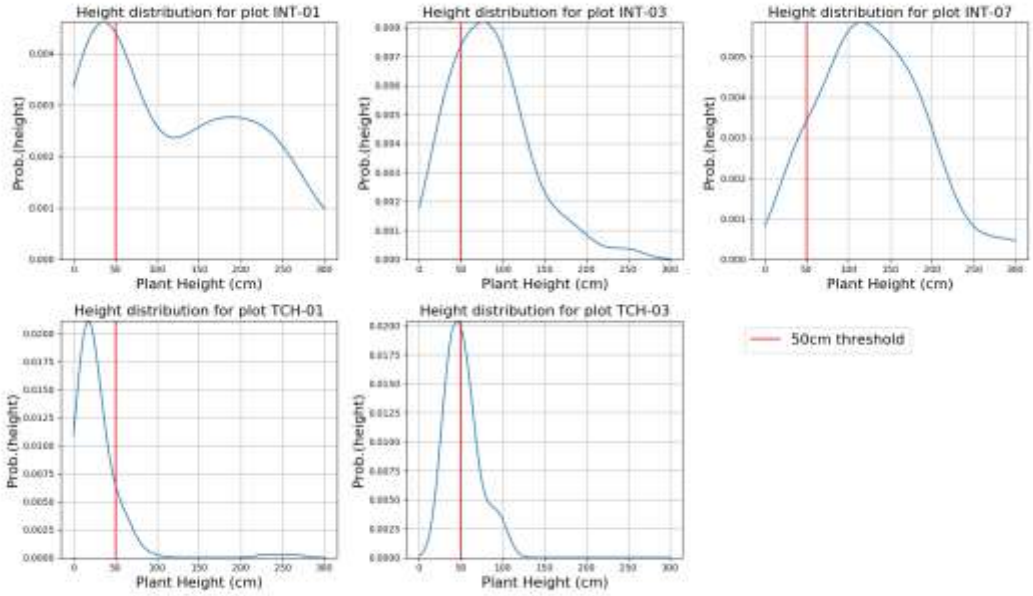


*Figure A.1 Height distributions per plot*

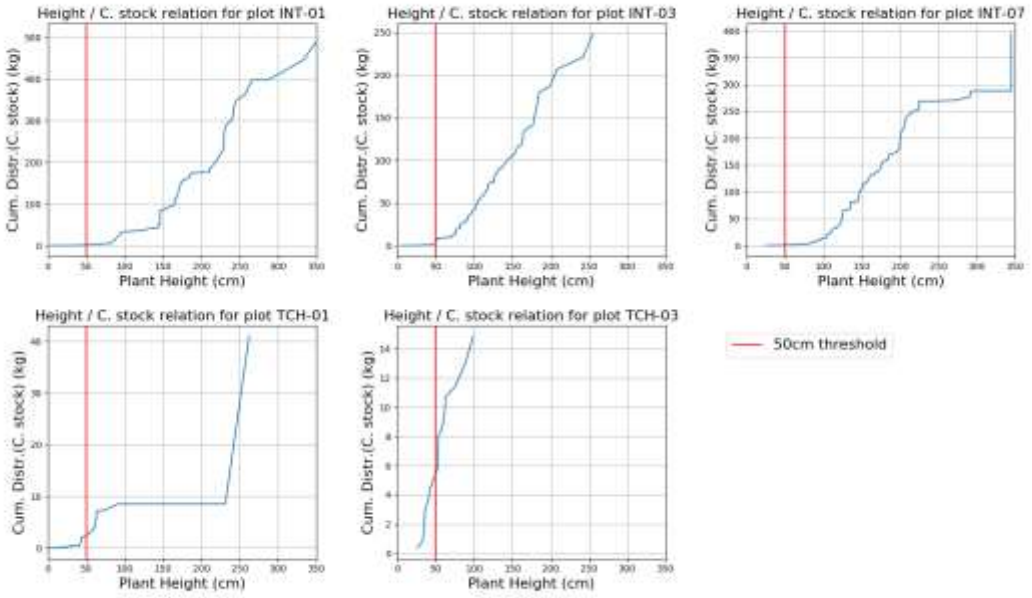


*Figure A.2 Carbon stock cumulative contributions by plant height*

Figure A.1 and Figure A.2 are intended to inform the design of nested plots with a possible plant threshold height. Figure A.1 shows the plant height distribution for each plot. These are kernel density estimates (KDE). Plants under 50cm comprise a substantial portion of the records. Figure A.2 shows the quantity of carbon contributed by plants of different heights. These graphs display the cumulative carbon contributions ordered by plant height for each plot. For all plots except TCH-03, the carbon contributed by plants with heights under 50cm makes a very small contribution to overall carbon. For TCH-03, these smaller plants contribute about 40% of the total carbon. This plot, however, has the lowest total carbon overall, meaning the 40% contribution is relatively insignificant in terms of total carbon. I believe these results support the use of a nested plot design. While plants under 50cm form a substantial portion of the measurements, they contribute very little to total carbon. I suggest using a 5x5m nested plot, where all plants are measured, and then only measuring plants taller than 50cm in the rest of the containing plot. The carbon for plants under 50cm in the 5x5m nested plot can be extrapolated to the containing plot. The 5x5m size is a loose recommendation and could perhaps be made smaller. This analysis suggests the nested plots will be beneficial for both degraded and intact plots. Practically, however, it may not be easy to quickly judge plant height in dense intact thicket.

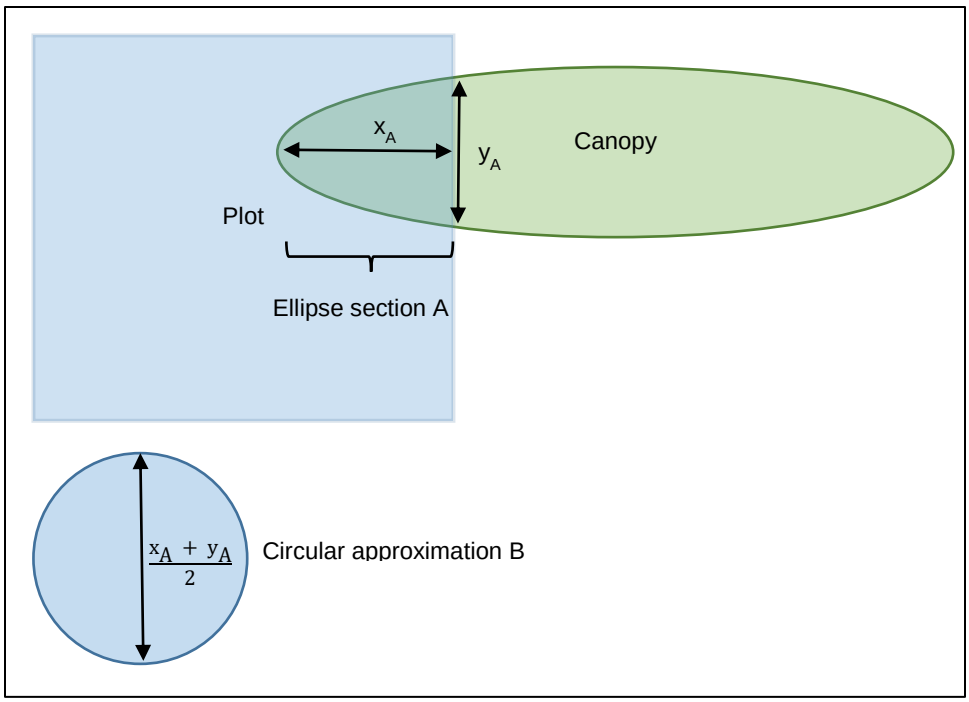


*Figure A.3 Edge intersected canopy area and approximation*

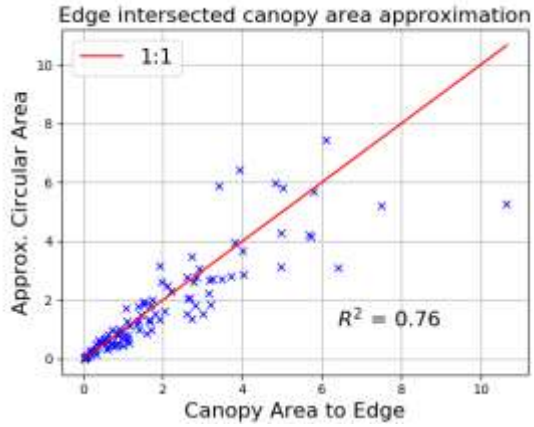


*Figure A.4 Edge intersected canopy area approximation*

Figure A.3 and Figure A.4 give a rough indication of how well canopy area can be approximated with a modified allometry approach, for the special case of plant canopy overlapping the plot boundary. Figure A.3 defines the areas being measured and approximated. Actual canopy is modelled by an ellipse that intersects the plot boundary to give the elliptical section area A. This area is approximated by the circular area B, which is effectively the standard allometric approach used in Marius' models. A number of randomly sized and positioned ellipses were generated and their corresponding intersected areas calculated as indicated in Figure A.3. Figure A.4 shows a scatter plot of area A versus the approximated area B for these ellipses. I think these results indicate that the approximation is acceptable.

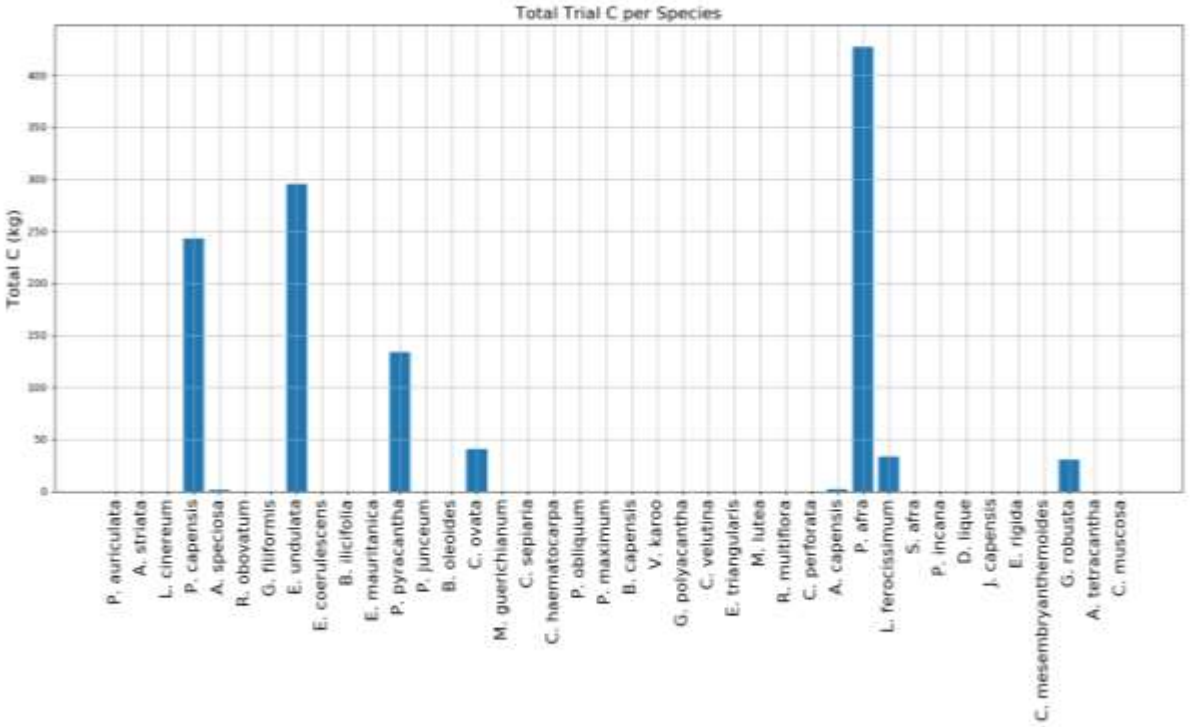


*Figure A.5 Total carbon per species over all plots*

Figure A.5 shows the total carbon contributed by each species over all of the trial plots. The four biggest contributors are *P. afra, E. undulata, P. capensis* and *P. pyracantha*.

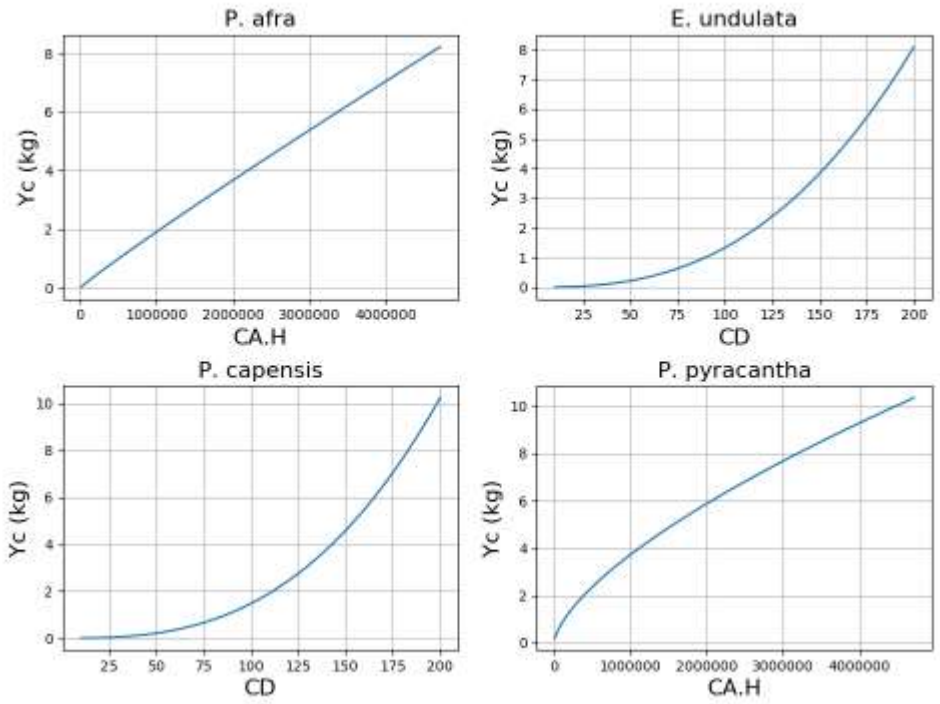


*Figure A.6 Carbon versus allometry for key species*

Figure A.6 shows how carbon (*Yc*) varies with the allometric measure (*x*) for each of the four key species' allometric models. See Marius' allometry table for further details of the models and their parameters. This plot was produced to give an indication of how linearly or otherwise carbon scales with plant dimension. It is (questionably) useful for informing the decision of how to treat plants overlapping the canopy boundary. E.g. if half the plant is overlapping and is measured, do we expect to get half the carbon from the allometric model?

My preference for treatment of plants overlapping the plot boundary is to measure them as indicated in Figure A.3. These results somewhat support this approach. I believe the strongest reason for this approach over others is a more conceptual one i.e. for degraded plots, containing possibly one or two large trees, it is likely to give the most accurate results. This is because it represents an appropriate portion of each tree rather than omitting or excluding it entirely.

## A.2 Dead Wood

Lying dead wood carbon stocks were estimated with Equation 6 from the CDM AR-Tool12 document (CDM 2015). Standing dead wood measurements were treated as lying dead wood and modelled as such, with Equation 6. It was not possible to apply specific CDM standing dead wood models, as only line transect diameter measurements were made during the trial (these models require height and stem diameter measurements to be made for dead wood inside the plot boundaries). The "default" carbon estimation approach of Equation 9 could also not be tested, as no default factor is available for arid habitats (see Section 8.1, Table 5 - (CDM 2015)).

The fixed parameters in Equation 6 were set as follows:

*Table A.1 Dead wood paramaters*

| Parameter | Description | Value |
|---|---|---|
| $\alpha_{PLOT}$ | Sample plot area (ha) | (10x10)/(100x100) = 0.01 |
| $CF_{TREE}$ | Carbon fraction of tree biomass (dimensionless) | 0.48 (Powell 2009) |
| $D_j$ | Basic wood density for species $j$ (t d.m.m$^{-3}$) | 0.5 for all species (estimate from dry-wet ratios in van der Vyver (2017)) |
| $L$ | Sum of lengths of the transects (m) | 100 |
| $\beta_n$ | Density reduction factor for n$^{th}$ piece of wood (dimensionless) | 1 for solid<br>0.8 for intermediate<br>0.45 for rotten<br>(CDM 2015) |

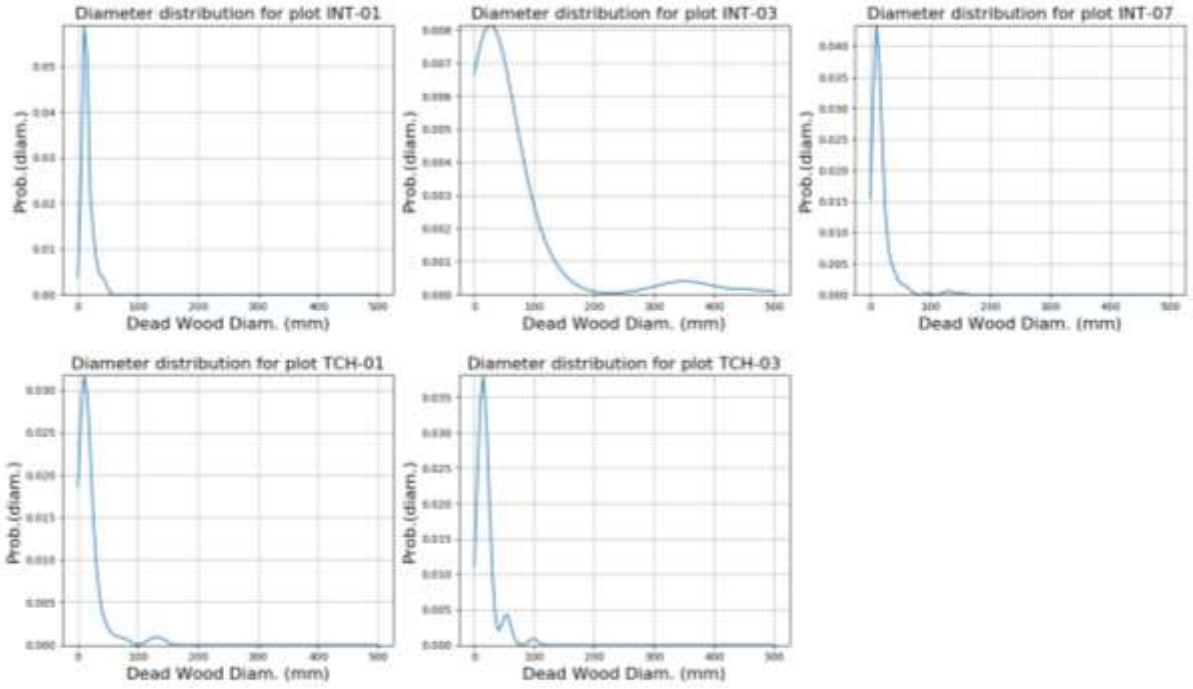


*Figure A.7 Dead wood diameter distributions per plot*

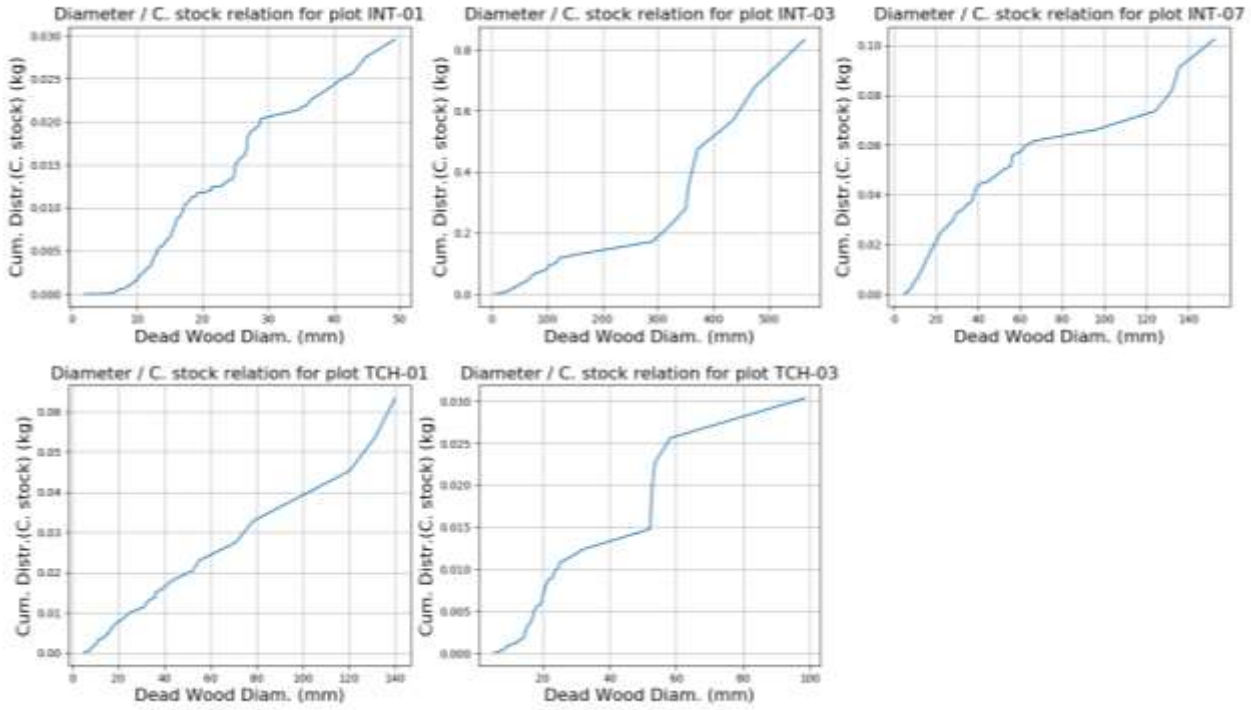


*Figure A.8 Carbon stock cumulative contributions by dead wood diameter*

Figure A.1 shows the dead wood diameter distribution for each plot. These are kernel density estimates (KDE). Diameters under 100mm comprise the majority of the records and 70% of measurements were made on diameters under 20mm. Figure A.2 shows the quantity of carbon contributed by dead wood of different diameters. These graphs display the cumulative carbon contributions ordered by diameter for each plot. The carbon is contributed fairly uniformly across the diameter range and there is not an obvious cut-off diameter for a possible nested approach. Nevertheless, limiting measurements to diameters above 20mm, would produce 95% of the dead wood carbon as measured in the trial (while reducing measurements by 70%).

Overall, the dead wood contributes a small fraction to total above-ground carbon (for comparison, see Figure A.2 for the woody canopy contributions of these plots). The highest dead wood contribution occurs in INT-03 where it produces about 0.3% of the above-ground carbon. With that in mind, I believe we could exclude the dead wood measurements from the methodology without significantly impacting on measurement accuracy.